

The recent warming trend in North Greenland

Anais Orsi, Kenji Kawamura, Valerie Masson-Delmotte, Xavier Fettweis, Jason Box, Dorthe Dahl-Jensen, Gary Clow, Amaelle Landais, Jeffrey Severinghaus

▶ **To cite this version:**

Anais Orsi, Kenji Kawamura, Valerie Masson-Delmotte, Xavier Fettweis, Jason Box, et al.. The recent warming trend in North Greenland. Geophysical Research Letters, 2017, 44 (12), pp.6235-6243. 10.1002/2016GL072212 . hal-03103991

HAL Id: hal-03103991
https://hal.science/hal-03103991

Submitted on 11 Jan 2021

HAL is a multi-disciplinary open access archive for the deposit and dissemination of scientific research documents, whether they are published or not. The documents may come from teaching and research institutions in France or abroad, or from public or private research centers.

L'archive ouverte pluridisciplinaire **HAL**, est destinée au dépôt et à la diffusion de documents scientifiques de niveau recherche, publiés ou non, émanant des établissements d'enseignement et de recherche français ou étrangers, des laboratoires publics ou privés.

AGU PUBLICATIONS

Geophysical Research Letters

RESEARCH LETTER
10.1002/2016GL072212

Special Section:
The Arctic: An AGU Joint Special Collection

The recent warming trend in North Greenland

Anais J. Orsi[1,2], Kenji Kawamura[3,4,5], Valerie Masson-Delmotte[2], Xavier Fettweis[6], Jason E. Box[7], Dorthe Dahl-Jensen[8], Gary D. Clow[9,10], Amaelle Landais[2], and Jeffrey P. Severinghaus[1]

[1]Scripps Institution of Oceanography, University of California, San Diego, La Jolla, California, USA, [2]Laboratoire des Sciences du Climat et de l'Environnement, LSCE/IPSL, CEA-CNRS-UVSQ, Université Paris-Saclay, Gif-sur-Yvette, France, [3]National Institute of Polar Research, Tokyo, Japan, [4]Department of Polar Science, Graduate University for Advanced Studies (SOKENDAI), Tokyo, Japan, [5]Institute of Biogeosciences, Japan Agency for Marine-Earth Science and Technology, Yokosuka, Japan, [6]Departement de Geographie, Universite de Liege, Liege, Belgium, [7]Geological Survey of Denmark and Greenland, Copenhagen, Denmark, [8]Centre for Ice and Climate, Niels Bohr Institute, University of Copenhagen, Copenhagen, Denmark, [9]U.S. Geological Survey, Lakewood, Colorado, USA, [10]Institute of Arctic and Alpine Research, University of Colorado Boulder, Boulder, Colorado, USA

Abstract The Arctic is among the fastest warming regions on Earth, but it is also one with limited spatial coverage of multidecadal instrumental surface air temperature measurements. Consequently, atmospheric reanalyses are relatively unconstrained in this region, resulting in a large spread of estimated 30 year recent warming trends, which limits their use to investigate the mechanisms responsible for this trend. Here we present a surface temperature reconstruction over 1982–2011 at NEEM (North Greenland Eemian Ice Drilling Project, 51°W, 77°N), in North Greenland, based on the inversion of borehole temperature and inert gas isotope data. We find that NEEM has warmed by 2.7 ± 0.33°C over the past 30 years, from the long-term 1900–1970 average of −28.55 ± 0.29°C. The warming trend is principally caused by an increase in downward longwave heat flux. Atmospheric reanalyses underestimate this trend by 17%, underlining the need for more in situ observations to validate reanalyses.

Key Points:
- NEEM (North West Greenland) has been warming by 2.7 plus/minus 0.3°C over 1982-2011
- The 30 year warm anomaly is exceptional in the context of the past 230 years
- The trend is principally caused by an increase in downward longwave heat flux

Supporting Information:
- Supporting Information S1
- Data Set S1

Correspondence to:
A. J. Orsi,
anais.orsi@lsce.ipsl.fr

Citation:
Orsi, A. J., K. Kawamura, V. Masson-Delmotte, X. Fettweis, J. E. Box, D. Dahl-Jensen, G. D. Clow, A. Landais, and J. P. Severinghaus (2017), The recent warming trend in North Greenland, *Geophys. Res. Lett.*, *44*, 6235–6243, doi:10.1002/2016GL072212.

Received 2 DEC 2016
Accepted 4 APR 2017
Accepted article online 17 APR 2017
Published online 28 JUN 2017

©2017. American Geophysical Union. All Rights Reserved.

1. Introduction

The Arctic region has warmed twice as much as the Northern Hemisphere over the past 30 years (1982–2011) [*Hansen et al.*, 2010; *Alexeev et al.*, 2012; *IPCC*, 2013] and is an important contributor to the observed global warming trend. The surface warming trend is largest in places where sea ice is disappearing (e.g., the Baffin Bay) and in coastal Greenland and Eastern Canada [*Hanna et al.*, 2012; *Vincent et al.*, 2012; *IPCC*, 2013].

The surface warming trend has been principally attributed to sea ice retreat and associated heat fluxes from the ocean [*Serreze et al.*, 2009; *Screen and Simmonds*, 2010a; , 2010b], to a negative trend in the North Atlantic Oscillation since 1990, increasing warm air advection on the West Coast of Greenland and Eastern Canada [*Hanna et al.*, 2012; *Fettweis et al.*, 2013; *Ding et al.*, 2014], and to an increase in the Greenland Blocking Index [*Hanna et al.*, 2013]. These latter mechanisms could be dominated by natural variability rather than forced response to the anthropogenic increase in greenhouse gases [*Fettweis et al.*, 2013; *Screen et al.*, 2014]. Teasing out mechanisms responsible for these anomalies requires a reasonable spatial coverage. In particular, it is important to resolve the east-west gradients to characterize circulation changes [e.g., *Ortega et al.*, 2014]. Additionally, it is useful to compare the recent trend with longer records to assess the significance of the observed changes. Regrettably, the meteorological data coverage is short and sparse in this region [*Cappelen et al.*, 2011; *Hanna et al.*, 2012; *Mernild et al.*, 2014]. Virtually all long time series are located on the coast (Figure 1). This limited spatiotemporal information prevents us from having a solid baseline on which to benchmark the recent warming trend and estimate whether the observed trend is out of the range of natural variability. Several studies have relied on atmospheric reanalyses to circumvent these limitations, using reanalyses to investigate mechanisms of multidecadal warming, and to produce Arctic temperature estimates from sparse observations [e.g., *Hansen et al.*, 2010; *Screen and Simmonds*, 2010a]. Above the Greenland ice sheet, the sparsity of meteorological observations is insufficient to characterize the spatial variability. Consequently, reanalyses are unlikely to be well constrained by existing observations. Indeed, we observe a large spread in

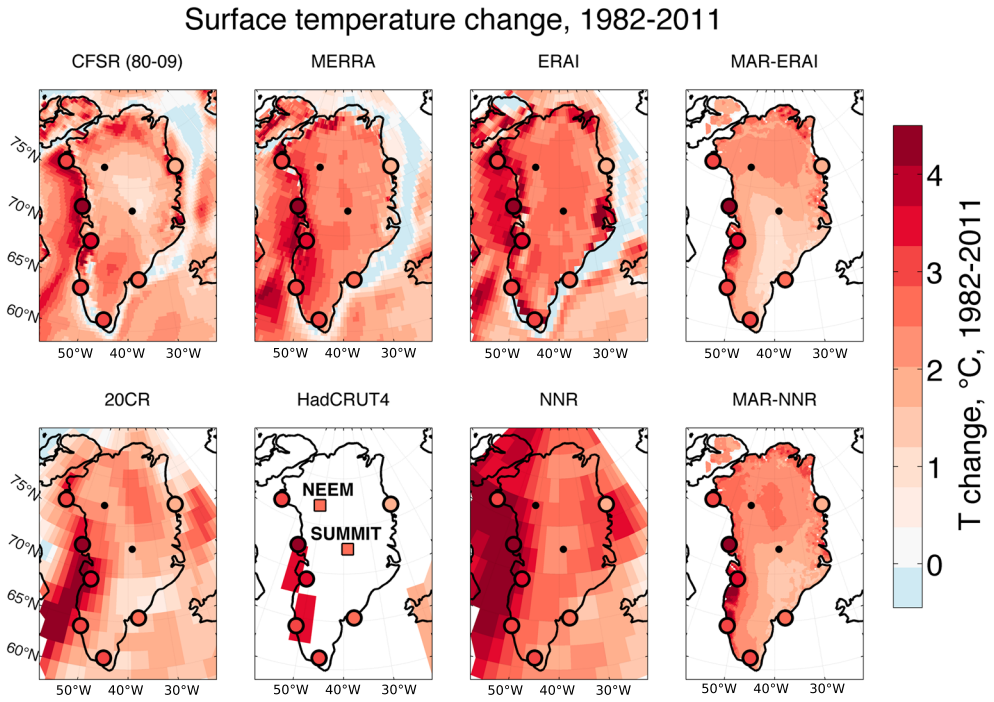


Figure 1. Thirty-year (1982–2011) surface temperature change from various reanalyses: NCEP-CFSR [*Saha et al.*, 2010], NASA-MERRA [*Rienecker et al.*, 2011], ERA-interim [*Dee et al.*, 2011], NCEP-20CR-v2c [*Compo et al.*, 2011], NCEP-NCAR reanalysis (NNR) [*Kalnay et al.*, 1996; *Kistler et al.*, 2001], as well as the outputs of the regional model MAR forced by either ERA-Interim or NNR [*Fettweis et al.*, 2013], and the surface temperature reconstruction from HadCRUT4 [*Morice et al.*, 2012]. The circles are trends calculated from all available weather stations having continuous measurements over the time period 1982–2011 [*Cappelen*, 2014]. The squares show the 30 year warming trend at NEEM (this work) and at Summit [*McGrath et al.*, 2013], the latter being based on the combination of firn temperatures and weather station data.

the estimates of the warming trend of the last 30 years (Figure 1), which questions the use of reanalyses to characterize the mechanisms responsible for the observed changes.

Here we present a temperature reconstruction from NEEM (North Greenland Eemian Ice Drilling Project, 51°W, 77°N), in North West Greenland, a region without long-term weather observations. We combined borehole temperature and inert gas isotope measurements in the firn, to produce the first homogenous 30 year observation of temperature above the Greenland ice sheet. The borehole temperature method is not subject to changes in calibration and is an ideal data set to estimate the surface temperature trend. NEEM is located away from the coast, at 2450 m altitude, where local albedo changes are small [*He et al.*, 2013; *Stroeve et al.*, 2013], and this site allows us to quantify the warming trend in a location primarily sensitive to warm air advection and associated longwave feedbacks (Figure S8 in the supporting information) [*Fettweis et al.*, 2013].

The data and methods are presented in section 2. Section 3 details the results. In section 4, we use $\delta^{18}O$ data to place the recent trend in the context of the past 270 years. In section 5, we compare the trend at NEEM with that of other stations in Greenland, and in section 6, we compare our reconstruction with atmospheric reanalyses.

2. Measurements and Methods

Snow and ice borehole temperature measurements take advantage of the low thermal conductivity of the snow and the high heat capacity of the ice, which allows the temperature history to be preserved in the ice for several centuries (section 2.1). In addition, we measured the isotopes of inert gases (N_2, Ar, and Kr), which have a constant atmospheric composition through time, and use the thermal fractionation signal as an additional constraint on the temperature history at the site (section 2.2). The inert gas data provide an independent estimation of the firn temperature profile. These two data sets are inverted to produce a robust temperature reconstruction (section 2.3), with a clear representation of uncertainties (section 2.4).

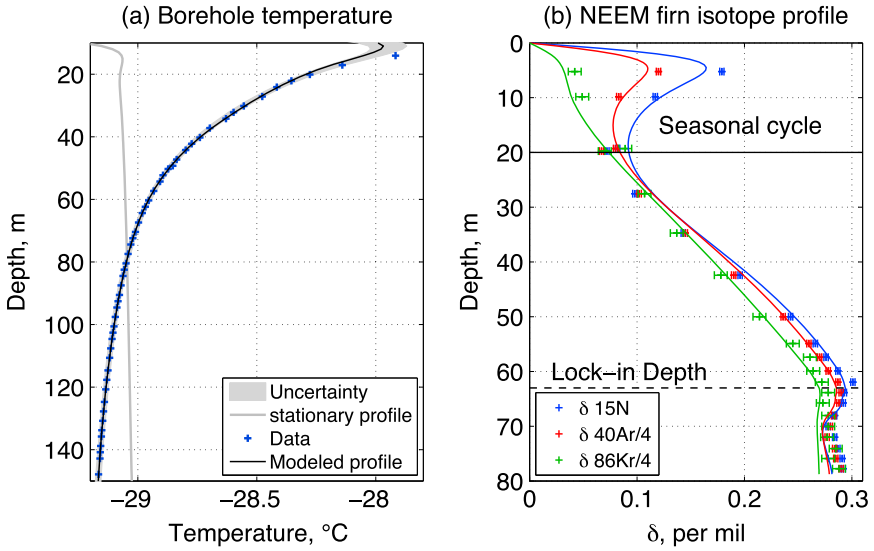


Figure 2. (a) Borehole temperature profile (+), with modeled fit to the data. A stationary temperature profile is shown in grey (run for 20 ka at −29.2°C). The temperature increase toward the surface indicates a warming trend. (b) Inert gas isotope data (+) and model fit (lines) from our best solution. The top 20 m signal shows the response to the seasonal cycle. Krypton isotopes (green) are the least sensitive to temperature and a good proxy for gravitational fractionation. The deviation between nitrogen isotopes (blue) and krypton isotopes (green) is the thermal signal. The lock-in depth is the horizon where advection dominates gas transport, and gravitational fractionation effectively stops.

2.1. Borehole Temperature Measurements

The temperature was measured in the NEEM2009S1 borehole in 2011 (2 years after drilling) to 147 m depth (Figure 2), using the method of *Orsi et al.* [2012]. The measurement precision is 2 mK below 50 m, and 20 mK above 50 m, estimated from repeat upward and downward logs. The lower precision toward the surface is due to the presence of a steeper gradient and small air motions in the borehole from surface wind.

The borehole temperature profile shows an increase of 1.5°C between 147 m depth and the surface, which directly indicates a warming trend (Figure 2).

2.2. Inert Gas Isotope Measurements

In addition, we measured the isotopic composition of N_2, Ar, and Kr in air pumped from the NEEM firn during 14–30 July 2008 from two boreholes: NEEM2008S1 and NEEM2008S2 [*Buizert et al.*, 2012]. We analyzed samples from 48 flasks, covering 22 depths. Samples were analyzed for nitrogen, argon, and krypton isotopes at Scripps Institution of Oceanography. Nitrogen isotopes were measured on dry air samples on a MAT-DeltaPlusXP following *Petrenko et al.* [2006]. Samples for Ar and Kr isotopes were extracted using a Zr/Al getter, which destroys all reactive gases and measured on a MAT-252 following *Orsi* [2013] and *Kawamura et al.* [2013]. The precision of the measurements was estimated by calculating the pooled standard deviation of replicate measurements from the same depths. It is respectively 0.012‰ for δ^{40}Ar, 0.036‰ for δ^{86}Kr, and 0.002‰ for δ^{15}N (Figure 2).

The linear increase in δ values with depth is due to gravitational fractionation, which is proportional to the depth in the firn, and to the mass difference between isotope pairs [*Sowers et al.*, 1989]. For simplicity, we have plotted δ values per unit mass difference Δm ($\Delta m = 1$ for $\delta^{15}N/^{14}N$, $\Delta m = 4$ for both $\delta^{40}Ar/^{36}Ar$, and $\delta^{86}Kr/^{82}Kr$), so that gravitational fractionation appears equal for all species. The difference between species at the same depth is due to thermal fractionation. Within the top 20 m, the large enrichment in δ^{15}N compared with δ^{86}Kr and δ^{40}Ar at the same depth is due to the strong temperature gradient resulting from the fact that the samples were taken in summer. N_2 is more sensitive to temperature than Ar and Kr, and heavy isotopes (high δ^{15}N) will concentrate in the cold portion of the firn. The difference between δ^{15}N and δ^{86}Kr in the deep firn signifies that the firn is colder than the surface, or in other words, that the surface has warmed.

These measurements document the impact of the surface warming trend on interstitial air for the first time. In earlier studies, the magnitude of recent temperature trends precluded the detection of a significant signal from inert gas isotopes. While these measurements do not add information to the borehole temperature

profile, because gases merely respond to firn temperature gradients, they provide an independent verification of the magnitude of the temperature gradient in the firn. These measurements also provide a verification of thermal fractionation theory, which has been used to interpret ice core measurements [e.g., *Severinghaus et al.*, 1998], but had never been observed in modern firn.

2.3. Model

We used a model of temperature diffusion [*Orsi et al.*, 2012] and of gas diffusion in the firn [*Severinghaus et al.*, 2010; *Buizert et al.*, 2012] to link the surface temperature history to a profile of temperature and inert gas isotopic composition. Details about the forward model are given in the supporting information [*Cuffey et al.*, 1994; *Rommelaere et al.*, 1997; *Goujon et al.*, 2003; *Grachev and Severinghaus*, 2003a, 2003b; *Cuffey and Paterson*, 2010]. In a nutshell, the forward model will take the temperature history $T_0(t)$ as an input, and output a temperature profile $T(z)$, and the inert gas isotopic composition ($\delta^{15}N(z)$, $\delta^{40}Ar(z)$ and $\delta^{86}Kr(z)$) through the firn. We can represent the forward model as $\mathfrak{M}$ and write

$$\left[T(z), \delta^{15}\mathrm{N}(z), \delta^{40}\mathrm{Ar}(z), \delta^{86}\mathrm{Kr}(z)\right] = \mathfrak{M}(T_0(t)) \quad (1)$$

We solve the inverse problem using linearized least squares with a basis of piecewise linear functions $T_i(t)$. The forward model is described by its response to basis functions, in a matrix form, and this matrix is inverted to retrieve the temperature history $T_0(t)$. The applicability of this method is detailed in *Orsi et al.* [2012] and described in the supporting information [*Wunsch*, 1996; *El Akkraoui et al.*, 2008; *Orsi et al.*, 2014].

The underdetermined nature of the inverse problem forces us to choose what we consider to be the "best" solution: we favor a solution with the smallest amount of change from a constant temperature history, and we favor a slow change of small amplitude rather than a faster change with a larger amplitude. Consequently, the results given here are a minimum estimate of the rate of warming compatible with the observations.

2.4. Uncertainty Estimation

The least squares inversion allows us to precisely quantify the uncertainty in the reconstruction by explicitly calculating the kernel of $\mathfrak{M}$: finding $T_k(t)$, so that $\mathfrak{M}(T_0(t)+T_k(t)) = \mathfrak{M}(T_0(t))$. We built a series of 1000 solutions to equation (1) by adding $T_k(t)$ to our best solution $T_0(t) : T_i(t) = T_0(t)+r_iT_k(t)$, using random numbers r_i of zero mean and unit variance. We then use these many $T_i(t)$ to quantify the uncertainty in our reconstruction. This approach includes both uncertainty due to model-data misfit (either due to measurement uncertainty or to the model's inability to resolve the fine structure in the data), and the uncertainty due to the underdetermined nature of the problem. It does not include uncertainties in model parameters that are not inverted for, such as boundary conditions, but the simulation length was long enough (1000 years) to avoid sensitivity to the initial condition (Figure S1). The sensitivity to other parameters (thermal diffusivity, vertical velocity, etc.) is small [*Muto*, 2010; *Orsi et al.*, 2012].

3. Temperature Reconstruction

We find that the past 30 years have been warming significantly, and that the resolution of our data is limited to the last 30 years (Figure 3). The warming rate is calculated as the slope of a linear regression for the period (1982–2011), on 1000 solutions to the inverse problem (section 2.4), and quoted in the following are the mean and standard deviation of these 1000 estimations. The warming rate for the period 1982–2011 is 0.91 ± 0.21°C/decade (Figure 5), or 2.7 ± 0.6°C warming over the past 30 years, which is one of the largest recorded on Earth, and 6 times the global average of 0.15°C/decade during this period [*McGrath et al.*, 2013]. We find that the last 30 year average is 0.71 ± 0.48°C warmer than the period 1950–1980 and 0.68 ± 0.56°C warmer than the period 1920–1950. The effective age distribution of a point in our temperature reconstruction is shown at the bottom of Figure 3 for several points in time. For instance, the width of the age distribution at half maximum is 8 years for the year 2000, 31 years for 1981, 60 years for 1960, and 120 years for 1940, which explains why the reconstruction for the first half of the twentieth century appears very flat (see supporting information Figure S7). We find that the last three decades have been increasingly warmer: the decade 1980–1990 is -0.1 ± 0.62°C, the decade 1990–2000 is 0.60 ± 0.40°C, and the decade 2000–2010 is 1.77 ± 0.33°C warmer than the long-term 1900–1970 average.

4. Is it Unprecedented?

In order to compare temperature changes during the last decades with earlier variations, we now rely on water stable isotopes from a composite of four shallow ice cores at the NEEM site [*Masson-Delmotte et al.*, 2015].

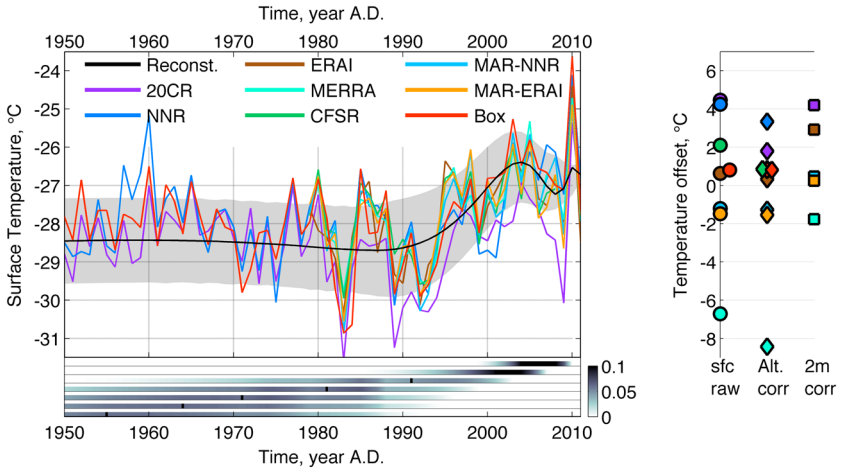


Figure 3. (left) Surface temperature reconstruction, from this inversion of borehole data and from a suite of atmospheric reanalyses: NCEP-20CR [*Compo et al.*, 2011], NCEP-NCAR [*Kalnay et al.*, 1996; *Kistler et al.*, 2001], ERA-interim [*Dee et al.*, 2011], NASA-MERRA [*Rienecker et al.*, 2011], and NCEP-CFSR [*Saha et al.*, 2010], as well as the outputs of the regional model MAR forced by either NCEP-NCAR or ERA-Interim [*Fettweis et al.*, 2013] and an interpolation of weather station data from *Box* [2013]. (right) A constant temperature offset was used on each data set to match the absolute temperature (1982–2011 mean) measured in the NEEM borehole. The circles depict the raw offset between modeled surface temperature and borehole temperature, the diamonds show the offset after correcting the surface elevation bias (Alt. Corr), and the squares show the elevation-corrected bias in 2 m (3 m for MAR) temperature. The bottom bars show the age distributions of our reconstruction at several points in time. Before 1980, the reconstructed temperature is the average of many decades, which makes the curve look flat.

Water isotopes (δ^{18}O) are affected by local temperature, and also other aspects of the atmospheric water cycle, such as moisture origin and precipitation intermittency. Although δ^{18}O is not a pure temperature proxy, it gives us an indication of similar climatic conditions in the past. We find that δ^{18}O has been increasing over the past 30 years, and that the decade 1996–2005 is the second highest decade in the 287 year record (Figure 4). The highest δ^{18}O values were found in 1928, which is also an extreme year in GISP2 (Greenland Ice Sheet Project 2) and NGRIP (North Greenland Ice core Project) ice cores, and in a coastal South Greenland composite [*Vinther et al.*, 2006; *Masson-Delmotte et al.*, 2015], but the decadal average (1926–1935) is not statistically different from the decade (2002–2011) (two sampled *t* test *p* value above 0.8). The 30 year average (1982–2011) is the highest of the record (Figure 4) but cannot be considered to be significantly higher than most of the

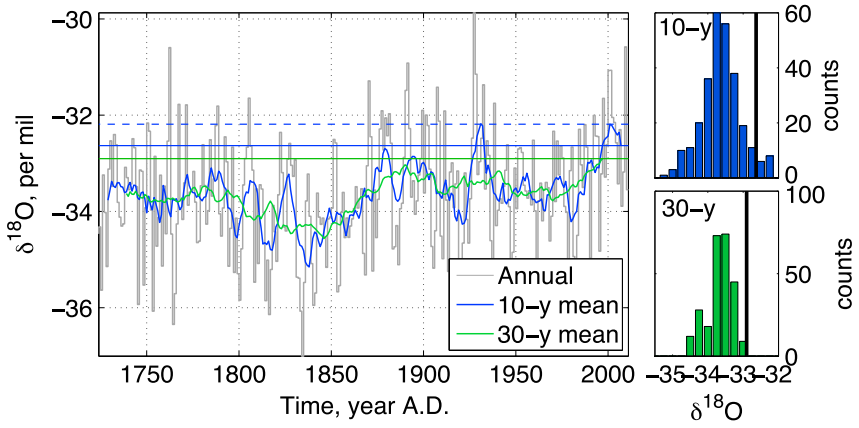


Figure 4. δ^{18}O in a composite of four shallow ice cores from NEEM [*Masson-Delmotte et al.*, 2015]. Annual mean (grey), 10 year running mean (blue), and 30 year running mean (green). The blue and green horizontal bars show the last 10 year mean and the last 30 year mean. Histograms on the right show the distribution to 10 (blue) and 30 year (green) temperature anomalies, and the most recent interval with a black bar. The recent warmest decade (1996–2005, dashed blue line) was superseded once in the last 287 years and is due to the large positive anomaly in 1928. The last 30 years are the warmest in the past 287 years.

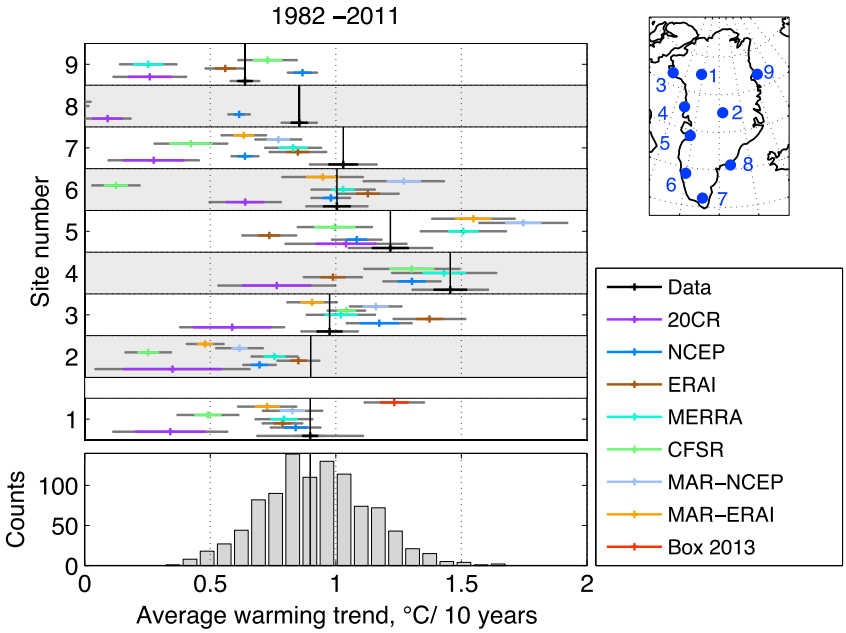


Figure 5. (bottom) Histogram of the calculated warming rate at NEEM (1) for the period 1982–2011. We find a warming of 0.91 ± 0.21°C/decade. (top) Warming rate from weather station data [*Cappelen*, 2014] (3, Pituffik; 4, Upernavik; 5, Ilulissat; 6, Nuuk; 7, Mittarfik; 8, Tasiilaq; and 9, Danmarkshavn) and Summit (2) [*McGrath et al.*, 2013] are shown in black, and reanalysis outputs at the corresponding grid point. The trend at NEEM is similar to that of Summit and other Greenland coastal sites (3, 6, 7, and 8).

twentieth century at the 0.05 level (see supporting information for details [*Benjamini and Hochberg*, 1995]). These observations indicate that NEEM is experiencing a prolonged warm period at the level of the warmest anomalies of the past 280 years.

5. Spatial Pattern of the Warming Trend

The last 30 year warming rate at NEEM has a very similar amplitude to that at other Greenland sites. We compared our record with long-term Danish Meteorological Institute coastal weather stations [Figure 5, *Hanna et al.*, 2012; *Cappelen*, 2014] and to Summit, where a composite temperature record has been built [*McGrath et al.*, 2013]. The 30 year (1982–2011) trend was calculated on 7 year smoothed data to allow for a meaningful comparison with the smooth temperature reconstruction. The uncertainty in the slope shown in Figure 5 was calculated by taking randomly 5 out of the 30 years and calculating the standard deviation of the slope of 100 such truncated data sets (colors), and also by calculating the uncertainty in the slope determination (grey lines) (Details are in the supporting information).

The largest annual warming trends are found at Upernavik (site 4, 1.5°C/decade) and Illulisat (site 5: 1.2°C/decade). These two sites are located near a region of large sea ice retreat and associated increase in sea surface temperature (Figure 1) and heat flux from the ocean to the atmosphere [*Serreze et al.*, 2009; *Screen and Simmonds*, 2010a, 2010b]. We find that NEEM (1), Summit (2), and coastal South Greenland (sites 6–8) have a similar warming rate over the past 30 years (1982–2011), even though changes in sea surface temperature, sea ice, and local snow cover may have specifically affected coastal sites, while this was not the case in the accumulation zone of the ice sheet (sites 1 and 2). This evidence points to the importance of changes in the large-scale circulation to the observed warming trend [*Hanna et al.*, 2012; *Fettweis et al.*, 2013; *Ding et al.*, 2014].

We examine the drivers of the surface temperature trend by investigating the surface energy balance at NEEM based on the regional model MAR forced by ERA-Interim reanalyses (Figure S8). MAR is a regional climate model run at 25 km resolution, with a specific surface transfer scheme adapted to snow, based on the snow model CROCUS [*Brun et al.*, 1992]. It has been extensively used to investigate Greenland surface mass balance [e.g., *Fettweis*, 2007; *Fettweis et al.*, 2011, 2013; *Tedesco et al.*, 2011, 2013, 2016]. MAR slightly underestimates the recent warming trend at NEEM (Figure 5), so the analysis presented here is likely to underestimate the trend in energy fluxes. We find that the simulated change in the energy budget at NEEM is dominated by

an increase in the downward longwave flux (+7.4 ± 0.3 W/m^2/30 years). Coastal Greenland sites are equally affected by an increasing downward longwave flux (e.g., +6.5 W/m^2/30 years at Nuuk, site 6), but the energy budget is also affected by an increase in downward shortwave flux (+4.3 W/m^2/30 years at Nuuk) linked to a decrease in albedo. The increase in downward longwave flux is consistent with a number of recent studies showing that the poleward moisture transport has been increasing, causing an increase in the greenhouse effect and, hence, warming [*Mattingly et al.*, 2016; *Woods and Caballero*, 2016; *Zhang et al.*, 2013; *Graversen and Burtu*, 2016; *Mortin et al.*, 2016]. It shows that longwave feedbacks play a significant role in the recent Greenland warming trend.

6. Comparison of Greenland Continental Temperature With Atmospheric Reanalyses

Atmospheric reanalyses provide the best estimate of three-dimensional climate evolution compatible with both observations and model physics and are an invaluable tool to investigate the potential mechanisms responsible for the observed warming trend. In central Greenland, there are very few data assimilated into the models [e.g., *Simmons and Poli*, 2015, Figure 6], and as a result, atmospheric models are relatively unconstrained and produce different simulations (Figure 1). We compare our time series to surface temperature estimations from a series of reanalysis data sets: NCEP-20CR [*Compo et al.*, 2011], NCEP-NCAR (NNR) [*Kalnay et al.*, 1996; *Kistler et al.*, 2001], ERA-interim [*Dee et al.*, 2011], NASA-Modern-Era Retrospective Analysis for Research and Applications (MERRA) [*Rienecker et al.*, 2011], and National Centers for Environmental Prediction Climate Forecast System Reanalysis (NCEP-CFSR) [*Saha et al.*, 2010], as well as the outputs of the regional model MAR forced by either NCEP-NCAR or ERA-Interim [*Fettweis et al.*, 2013] and the weather station interpolation of *Box* [2013].

We estimated the bias in reanalyses and simulations by comparing the 30 year mean (1982–2011) to our temperature reconstruction, which is an absolute temperature measurement (Figure 3, right). We find that 20CR, NCEP-NCAR, and NCEP-CFSR have significant warm biases, which are partly due to a bias in topography. The diamonds in Figure 3 show the bias, corrected for altitude, using a lapse rate of 7°C/km [*Steffen and Box*, 2001]. MERRA has a significant cold bias (−6.7°C) at the surface, but less than −1.8°C at 2 m, showing that the surface inversion is likely too strong in the model. The model MAR has a slight negative bias (−1.5°C) at the surface but near zero bias at 2 m. The use of the regional model MAR significantly decreases the warm bias (Figure 3) in NCEP-NCAR, showing the sensitivity of the surface temperature bias to model resolution and surface physics.

The temperature trend at NEEM is consistently lower in the reanalyses than in our reconstruction (Figure 5): the trend computed from reanalyses has a mean of 0.74 ± 0.13°C/decade, against 0.91 ± 0.21°C/decade in our estimate. A stronger mismatch is identified for Summit, (Figure 5, site 2), where the reanalyses predict on average a trend of 0.61 ± 0.21°C/decade (excluding 20CR), and observations have a trend of 0.94 ± 0.13°C/decade. This discrepancy is possibly due to an overestimation of surface temperature inversion strength and frequency in reanalyses. Indeed, ERA-Interim, for instance, overestimates wintertime inversion frequency [*Zhang et al.*, 2011], a feature that is shared by most Coupled Model Intercomparison Project Phase 5 atmospheric climate models [*Boe et al.*, 2009; *Medeiros et al.*, 2011], which greatly impacts the surface temperature evolution.

These observations show the limits of inferring the long-term surface temperature trend of the Greenland ice sheet from the current generation of atmospheric reanalyses and identifying the mechanisms responsible for this trend. It is essential to improve the observations of the vertical temperature and humidity profiles in continental Greenland to better constrain the response of the polar boundary layer to global warming and model the future evolution of the Greenland ice sheet.

7. Conclusion

We measured borehole temperature and inert gas isotope data to reconstruct the surface temperature history at NEEM, in central North Greenland. We found that the past 30 years (1982–2011) have been warming at a rate of 0.91 ± 0.21°C/decade. δ^{18}O data indicate that the warmth of the last 30 years is at the level of the warmest anomalies of the last 280 years. The warming rate at NEEM is similar to that of Greenland Summit, and to coastal weather stations, demonstrating that the surface warming trend is widespread and not limited to coastal regions directly affected by albedo and sea ice changes. It is associated with a +7.4 ± 0.3 W/m^2/30 years

increase in downward longwave flux according to MAR-ERAI, which is consistent with the observed increase in poleward moisture transport to the Arctic. Atmospheric reanalyses underestimate the 30 year trend by 17% at NEEM and 35% at Summit, which suggest that models may not properly capture mechanisms of amplified warming above the Greenland ice sheet. This finding calls for an improvement of observations of the vertical temperature and humidity profiles in continental Greenland to better constrain the response of the polar boundary layer to global warming.

Acknowledgments

NEEM is directed and organized by the Center of Ice and Climate at the Niels Bohr Institute and U.S. NSF, Office of Polar Programs. It is supported by funding agencies and institutions in Belgium (FNRS-CFB and FWO), Canada (NRCan/GSC), China (CAS), Denmark (FIST), France (IPEV, CNRS/INSU, CEA and ANR), Germany (AWI), Iceland (RannIs), Japan (NIPR), Korea (KOPRI), The Netherlands (NWO/ALW), Sweden (VR), Switzerland (SNF), United Kingdom (NERC), and the USA (U.S. NSF, Office of Polar Programs). V.M.D. acknowledges support by the French Agence Nationale de la Recherche (grant VMC NEEM and CEPS GREENLAND). A.O. was supported at SIO by NSF grant 08-06377 (to J.P.S) and at LSCE by a FP7 Marie Curie IIF (TALDICE-Holocene). K.K. acknowledges supports by JSPS (KAKENHI 21671001 and 26241011) and NIPR Advanced Research Project. G.D.C. was supported by the U.S. Geological Survey Climate and Land Use Change Program. Any use of trade, firm, or product names is for descriptive purposes only and does not imply endorsement by the U.S. Government. Supporting data are included in an SI file; any additional data may be obtained from A.J.O.

References

Alexeev, V. A., I. Esau, I. V. Polyakov, S. J. Byam, and S. Sorokina (2012), Vertical structure of recent Arctic warming from observed data and reanalysis products, *Clim. Change*, *111*(2), 215–239.

Benjamini, Y., and Y. Hochberg (1995), Controlling the false discovery rate: A practical and powerful approach to multiple testing, *J. R. Stat. Soc., Ser. B*, *57*, 289–300.

Boe, J., A. Hall, and X. Qu (2009), Current GCMs' unrealistic negative feedback in the Arctic, *J. Clim.*, *22*(17), 4682–4695.

Box, J. E. (2013), Greenland ice sheet mass balance reconstruction. Part II. Surface mass balance (1840-2010), *J. Clim.*, *26*(18), 6974–6989.

Brun, E., P. David, M. Sudul, and G. Brunot (1992), A numerical model to simulate snow-cover stratigraphy for operational avalanche forecasting, *J. Glaciol.*, *38*(128), 13–22.

Buizert, C., et al. (2012), Gas transport in firn: multiple-tracer characterisation and model intercomparison for NEEM, Northern Greenland Gas transport in firn: Multiple-tracer characterisation and model intercomparison for NEEM, Northern Greenland, *Atmos. Chem. Phys.*, *12*, 4259–4277.

Cappelen, J., (2014), Greenland - DMI historical climate data collection 1873–2013, *Tech. Rep. 14-04*, Danish Meteorol. Inst., Copenhagen.

Cappelen, J., E. V. Laursen, P. V. Jørgensen, and C. Kern-Hansen, (2011), DMI monthly climate data collection 1768–2010, Denmark, the Faroe Islands and Greenland, *Tech. Rep. 05-05*, Danish Meteorol. Inst., Copenhagen.

Compo, G. P. et al. (2011), The twentieth century reanalysis project, *Q. J. R. Meteorol. Soc.*, *137*(654), 1–28.

Cuffey, K., and W. Paterson (2010), *The Physics of Glaciers*, Academic Press, Amsterdam.

Cuffey, K., R. Alley, P. Grootes, J. Bolzan, and S. Anandakrishnan (1994), Calibration of the δ^{18}O isotopic paleothermometer for central Greenland, using borehole temperatures, *J. Glaciol.*, *40*(135), 341–349.

Dee, D., et al. (2011), The Era-Interim reanalysis: Configuration and performance of the data assimilation system, *Q. J. R. Meteorol. Soc.*, *137*(656), 553–597.

Ding, Q., J. M. Wallace, D. S. Battisti, E. J. Steig, A. J. E. Gallant, H.-J. Kim, and L. Geng (2014), Tropical forcing of the recent rapid arctic warming in northeastern Canada and Greenland, *Nature*, *509*(7499), 209–212.

El Akkraoui, A., P. Gauthier, S. Pellerin, and S. Buis (2008), Intercomparison of the primal and dual formulations of variational data assimilation, *Q. J. R. Meteorol. Soc.*, *134*(633), 1015–1025.

Fettweis, X. (2007), Reconstruction of the 1979? 2006 Greenland ice sheet surface mass balance using the regional climate model MAR, *Cryosphere*, *1*(1), 21–40.

Fettweis, X., M. Tedesco, M. Broeke, and J. Ettema (2011), Melting trends over the Greenland ice sheet (1958–2009) from spaceborne microwave data and regional climate models, *Cryosphere*, *5*(2), 359–375.

Fettweis, X., E. Hanna, C. Lang, A. Belleflamme, M. Erpicum, and H. Gallée (2013), Brief communication "Important role of the mid-tropospheric atmospheric circulation in the recent surface melt increase over the Greenland ice sheet", *Cryosphere*, *7*(1), 241–248.

Goujon, C., J. Barnola, and C. Ritz (2003), Modeling the densification of polar firn including heat diffusion: Application to close-off characteristics and gas isotopic fractionation for Antarctica and Greenland sites, *J. Geophys. Res.*, *108*(D24), 4792, doi:10.1029/2002JD003319.

Grachev, A., and J. Severinghaus (2003a), Laboratory determination of thermal diffusion constants for 29N2/28N2 in air at temperatures from −60 to 0°C for reconstruction of magnitudes of abrupt climate changes using the ice core fossil-air paleothermometer, *Geochim. Cosmochim. Acta*, *67*(3), 345–360.

Grachev, A., and J. Severinghaus (2003b), Determining the thermal diffusion factor for 40Ar/36Ar in air to aid paleoreconstruction of abrupt climate change, *J. Phys. Chem. A*, *107*, 4636–4642.

Graversen, R. G., and M. Burtu (2016), Arctic amplification enhanced by latent energy transport of atmospheric planetary waves, *Q. J. R. Meteorol. Soc.*, *142*(698), 2046–2054, doi:10.1002/qj.2802.

Hanna, E., S. H. Mernild, J. Cappelen, and K. Steffen (2012), Recent warming in Greenland in a long-term instrumental (1881–2012) climatic context: I. Evaluation of surface air temperature records, *Environ. Res. Lett.*, *7*(4), 045404.

Hanna, E., J. M. Jones, J. Cappelen, S. H. Mernild, L. Wood, K. Steffen, and P. Huybrechts (2013), The influence of North Atlantic atmospheric and oceanic forcing effects on 1900–2010 Greenland summer climate and ice melt/runoff, *Int. J. Climatol.*, *33*(4), 862–880.

Hansen, J., R. Ruedy, M. Sato, and K. Lo (2010), Global surface temperature change, *Rev. Geophys.*, *48*, RG4004, doi:10.1029/2010RG000345.

He, T., S. Liang, Y. Yu, D. Wang, F. Gao, and Q. Liu (2013), Greenland surface albedo changes in july 1981–2012 from satellite observations, *Environ. Res. Lett.*, *8*(4), 044043.

IPCC (2013), Summary for policymakers, in *Climate Change 2013: The Physical Science Basis. Contribution of Working Group I to the Fifth Assessment Report of the Intergovernmental Panel on Climate Change*, edited by T. F. Stocker et al., 1535 pp., Cambridge Univ. Press, Cambridge, U. K., and New York, doi:10.1017/CBO9781107415324.

Kalnay, E., et al. (1996), The NCEP/NCAR 40-year reanalysis project, *Bull. Am. Meteorol. Soc.*, *77*(3), 437–471.

Kawamura, K., J. P. Severinghaus, M. R. Albert, Z. R. Courville, M. A. Fahnestock, T. Scambos, E. Shields, and C. A. Shuman (2013), Kinetic fractionation of gases by deep air convection in polar firn, *Atmos. Chem. Phys.*, *13*(21), 11,141–11,155, doi:10.5194/acp-13-11141-2013.

Kistler, R., et al. (2001), The NCEP-NCAR 50-year reanalysis: Monthly means CD-ROM and documentation, *Bull. Am. Meteorol. Soc.*, *82*(2), 247–267.

Masson-Delmotte, V., et al. (2015), Recent changes in north-west Greenland climate documented by NEEM shallow ice core data and simulations, and implications for past-temperature reconstructions, *Cryosphere*, *9*(4), 1481–1504, doi:10.5194/tc-9-1481-2015.

Mattingly, K. S., C. A. Ramseyer, J. J. Rosen, T. L. Mote, and R. Muthyala (2016), Increasing water vapor transport to the Greenland ice sheet revealed using self-organizing maps, *Geophys. Res. Lett.*, *43*, 9250–9258, doi:10.1002/2016GL070424.

McGrath, D., W. Colgan, N. Bayou, A. Muto, and K. Steffen (2013), Recent warming at summit, Greenland: Global context and implications, *Geophys. Res. Lett.*, *40*, 2091–2096, doi:10.1002/grl.50456.

Medeiros, B., C. Deser, R. A. Tomas, and J. E. Kay (2011), Arctic inversion strength in climate models, *J. Clim.*, *24*(17), 4733–4740.

Mernild, S. H., E. Hanna, J. C. Yde, J. Cappelen, and J. K. Malmros (2014), Coastal Greenland air temperature extremes and trends 1890–2010: Annual and monthly analysis, *Int. J. Climatol.*, *34*(5), 1472–1487.
Morice, C. P., J. J. Kennedy, N. A. Rayner, and P. D. Jones (2012), Quantifying uncertainties in global and regional temperature change using an ensemble of observational estimates: The HadCRUT4 data set, *J. Geophys. Res.*, *117*, D08101, doi:10.1029/2011JD017187.
Mortin, J., G. Svensson, R. G. Graversen, M.-L. Kapsch, J. C. Stroeve, and L. N. Boisvert (2016), Melt onset over Arctic sea ice controlled by atmospheric moisture transport, *Geophys. Res. Lett.*, *43*, 6636–6642, doi:10.1002/2016GL069330.
Muto, A. (2010), Multi-decadal surface temperature trends in East Antarctica inferred from borehole firn temperature measurements and geophysical inverse methods, PhD thesis, Univ. of Colorado, Boulder, Colo.
Orsi, A., B. Cornuelle, and J. Severinghaus (2012), Little Ice Age cold interval in West Antarctica: Evidence from borehole temperature at the West Antarctic Ice Sheet (WAIS) divide, *Geophys. Res. Lett.*, *39*, L09710, doi:10.1029/2012GL051260.
Orsi, A. J. (2013), Temperature reconstruction at the West Antarctic Ice Sheet divide, for the last millennium, from the combination of borehole temperature and inert gas isotope measurements, PhD thesis, Univ. of California San Diego, La Jolla, Calif.
Orsi, A. J., B. D. Cornuelle, and J. P. Severinghaus (2014), Magnitude and temporal evolution of Dansgaard-Oeschger event 8 abrupt temperature change inferred from nitrogen and argon isotopes in GISP2 ice using a new least-squares inversion, *Earth Planet. Sci. Lett.*, *395*, 81–90, doi:10.1016/j.epsl.2014.03.030.
Ortega, P., D. Swingedouw, V. Masson-Delmotte, C. Risi, B. Vinther, P. Yiou, R. Vautard, and K. Yoshimura (2014), Characterizing atmospheric circulation signals in Greenland ice cores: Insights from a weather regime approach, *Clim. Dyn.*, *43*, 2585–2605.
Petrenko, V. V., J. P. Severinghaus, E. J. Brook, N. Reeh, and H. Schaefer (2006), Gas records from the West Greenland ice margin covering the last glacial termination: A horizontal ice core, *Quat. Sci. Rev.*, *25*(9), 865–875.
Rienecker, M. M., et al. (2011), MERRA: Nasa's Modern-Era Retrospective Analysis for Research and Applications, *J. Clim.*, *24*(14), 3624–3648.
Rommelaere, V., L. Arnaud, and J. Barnola (1997), Reconstructing recent atmospheric trace gas concentrations from polar firn and bubbly ice data by inverse methods, *J. Geophys. Res.*, *102*(D25), 30,069–30,083.
Saha, S., et al. (2010), The NCEP climate forecast system reanalysis, *Bull. Am. Meteorol. Soc.*, *91*(8), 1015–1057.
Screen, J. A., and I. Simmonds (2010a), The central role of diminishing sea ice in recent Arctic temperature amplification, *Nature*, *464*(7293), 1334–1337.
Screen, J. A., and I. Simmonds (2010b), Increasing fall-winter energy loss from the Arctic Ocean and its role in Arctic temperature amplification, *Geophys. Res. Lett.*, *37*, L16707, doi:10.1029/2010GL044136.
Screen, J. A., C. Deser, I. Simmonds, and R. Tomas (2014), Atmospheric impacts of Arctic sea-ice loss, 1979–2009: Separating forced change from atmospheric internal variability, *Clim. Dyn.*, *43*(1–2), 333–344.
Serreze, M., A. Barrett, J. Stroeve, D. Kindig, and M. Holland (2009), The emergence of surface-based Arctic amplification, *Cryosphere*, *3*(1), 11–19.
Severinghaus, J. P., T. Sowers, E. J. Brook, M. L. Bender, and R. B. Alley (1998), Timing of abrupt climate change at the end of the Younger Dryas interval from thermally fractionated gases in polar ice, *Nature*, *391*(6663), 141–146.
Severinghaus, J. P., et al. (2010), Deep air convection in the firn at a zero-accumulation site, central Antarctica, *Earth Planet. Sci. Lett.*, *293*(3–4), 359–367, doi:10.1016/j.epsl.2010.03.003.
Simmons, A. J., and P. Poli (2015), Arctic warming in Era-Interim and other analyses, *Q. J. R. Meteorol. Soc.*, *141*(689), 1147–1162.
Sowers, T., M. Bender, and D. Raynaud (1989), Elemental and isotopic composition of occluded O_2 and N_2 in polar ice, *J. Geophys. Res.*, *94*(D4), 5137–5150.
Steffen, K., and J. Box (2001), Surface climatology of the Greenland ice sheet: Greenland climate network 1995–1999, *J. Geophys. Res.*, *106*(D24), 33,951–33,964.
Stroeve, J., J. E. Box, Z. Wang, C. Schaaf, and A. Barrett (2013), Re-evaluation of MODIS MCD43 Greenland albedo accuracy and trends, *Remote Sens. Environ.*, *138*, 199–214.
Tedesco, M., X. Fettweis, M. Van den Broeke, R. Van de Wal, C. Smeets, W. J. van de Berg, M. Serreze, and J. Box (2011), The role of albedo and accumulation in the 2010 melting record in Greenland, *Environ. Res. Lett.*, *6*(1), 014005, doi:10.1088/1748-9326/6/1/014005.
Tedesco, M., X. Fettweis, T. Mote, J. Wahr, P. Alexander, J. Box, and B. Wouters (2013), Evidence and analysis of 2012 Greenland records from spaceborne observations, a regional climate model and reanalysis data, *Cryosphere*, *7*, 615–630.
Tedesco, M., T. Mote, X. Fettweis, E. Hanna, J. Jeyaratnam, J. Booth, R. Datta, and K. Briggs (2016), Arctic cut-off high drives the poleward shift of a new Greenland melting record, *Nat. Commun.*, *7*, 11723.
Vincent, L. A., X. L. Wang, E. J. Milewska, H. Wan, F. Yang, and V. Swail (2012), A second generation of homogenized Canadian monthly surface air temperature for climate trend analysis, *J. Geophys. Res.*, *117*, D18110, doi:10.1029/2012JD017859.
Vinther, B. M., K. K. Andersen, P. Jones, K. Briffa, and J. Cappelen (2006), Extending Greenland temperature records into the late eighteenth century, *J. Geophys. Res.*, *111*, D11105, doi:10.1029/2005JD006810.
Woods, C., and R. Caballero (2016), The role of moist intrusions in winter arctic warming and sea ice decline, *J. Clim.*, *29*(12), 4473–4485.
Wunsch, C. (1996), *The Ocean Circulation Inverse Problem*, Cambridge Univ. Press, Cambridge, U. K.
Zhang, X., J. He, J. Zhang, I. Polyakov, R. Gerdes, J. Inoue, and P. Wu (2013), Enhanced poleward moisture transport and amplified northern high-latitude wetting trend, *Nat. Clim. Change*, *3*(1), 47–51.
Zhang, Y., D. J. Seidel, J.-C. Golaz, C. Deser, and R. A. Tomas (2011), Climatological characteristics of Arctic and Antarctic surface-based inversions, *J. Clim.*, *24*(19), 5167–5186.